

The discharge rate of the capacitor is:

$$\frac{dV_{CW}}{dt} = \frac{-I_{D2}}{C_W} = \frac{-(I_{D3} + I_{D4})}{C_W} \quad (1)$$

where V_{CW} is the voltage across C_w , and I_{D3} and I_{D4} are the drain currents of M_3 and M_4 , which are in triode in most of the input voltage range. When ϕ_{clk} is high, M_2 is ON and $V_{DS3} = V_{DS4} \approx V_{CW}$. Therefore [9],

$$I_{D3} = \mu_n C_{ox} \frac{W_3}{L_3} \left((V_B - V_{tn}) V_{CW} - \frac{1}{2} V_{CW}^2 \right) \quad (2)$$

$$I_{D4} = \mu_n C_{ox} \frac{W_4}{L_4} \left((V_{DD} - V_{tn}) V_{CW} - \frac{1}{2} V_{CW}^2 \right) \quad (3)$$

where μ_n is the mobility of the carriers, C_{ox} is the gate oxide capacitance per unit area, W/L is the aspect ratio of the respective transistors and V_{tn} is the threshold voltage of NMOS transistors. Eq. (1) and (2) indicate how the voltage V_B changes the time constant of the discharging path and thus controls the delay of the output signal.

The time-difference interval between rising edges of ϕ_{clk} and ϕ_{out} is a representation of the input signal in the time domain. This time-difference is controlled by capacitor C_w , control voltage V_B , and transistors in the discharging path. This design is linear for an input voltage between 0.8 V to 1.2 V [4], the nonlinearity at lower input voltages being mainly caused by M_3 entering the subthreshold region.

In order to increase the linear input range of the VCDU, the signal conditioning circuit of Fig. 3 is proposed. This circuit improves the linearity range by two mechanisms. A DC offset is applied to the input voltage while the circuit has an exponential response in the midrange (from 0.5 V to 1.2 V). This is achieved by combining two voltage sources through transistors M_{12} and M_{13} . The DC offset is realized with the voltage divider formed by R_1 and R_2 and two NMOS transistors, M_{7-8} . The input voltage is increased through the diode-connected transistor M_8 and the gate-source of M_7 . This DC offset ensures that M_3 is in saturation at low input voltages. Finally, the combination of transistors M_{9-11} with the DC offset generates the desired exponential response in the midrange.

The transfer characteristics of the signal conditioning block is shown in Fig. 4, including the effect of a $\pm 1\%$ and $\pm 5\%$ mismatch on the value of R_1 . To our knowledge, this circuit is the first structure that applies transformations to the input signal to improve the linearity of TMSP circuits without using any operational amplifier.

III. SIMULATION RESULTS

The Taillefer VCDU [4] and the proposed VCDU were designed and simulated using Spectre in a TSMC 0.18 μm CMOS process with a 1.8 V supply voltage. Fig. 5 shows that the linear range of the VCDU was effectively extended using the proposed signal conditioning circuit, and that the conversion gain was also improved. For both VCDUs, the output data was exported to MATLAB, and a linear regression was performed to evaluate the linearity error.

Since a typical application of TMSP circuits is analog-to-digital conversion, we define the linear range of the VCDU as

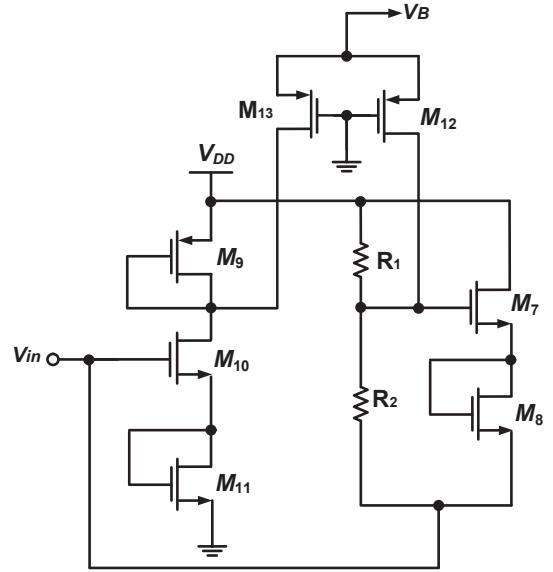


Fig. 3. Circuit diagram of the proposed signal conditioning block.

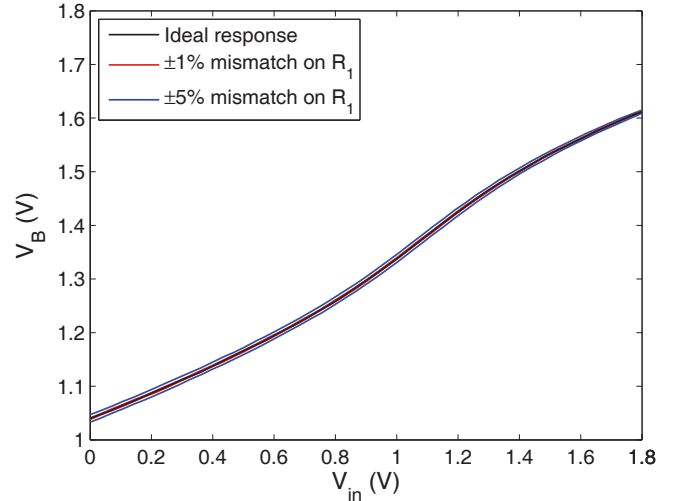


Fig. 4. DC response of the signal conditioning block.

the input range for which the linearity error is less than half the step of the least significant bit (LSB) for an 8-bit ADC. For this purpose, the following relative linearity error calculation is used:

$$\epsilon = \frac{E}{FS} * 100\% \quad (4)$$

where E is the largest deviation from the ideal (linear) behavior over the full scale linear range FS of input voltage. As shown in Fig. 6, the linear range which provides 8-bit resolution ($\pm 0.2\%$) for the proposed VCDU is from 0.15 V to 1 V, which is suitable for low-voltage TMSP.

One of the anticipated issue with the proposed signal conditioning circuit is the sensitivity to the ratio of the values of resistors R_1 and R_2 . To evaluate this sensitivity, simulations were performed by forcing a 1% error on the value of R_1 . Fig. 6 shows that the linearity error was not affected by this mismatch on R_1 and R_2 , i.e. the linear range for 8-bit

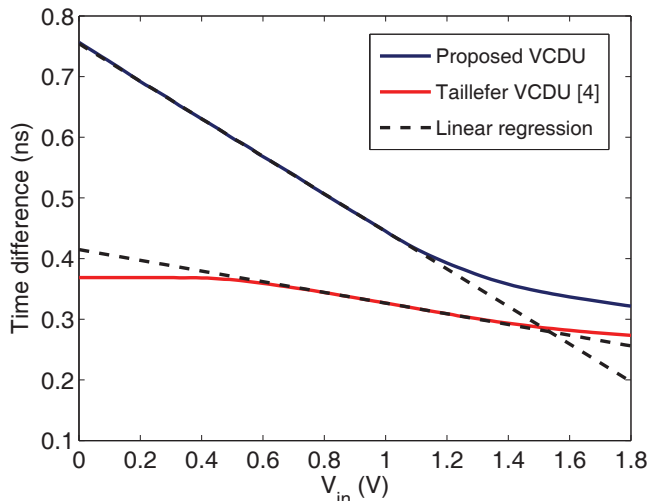


Fig. 5. Transfer characteristic of Taillefer VCDU and proposed VCDU.

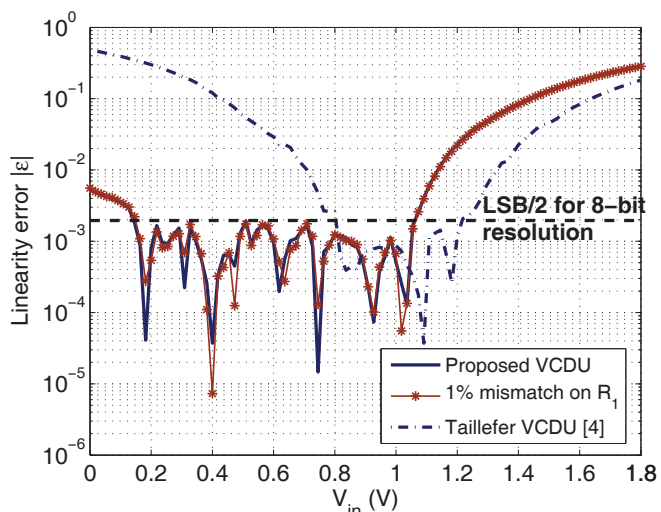


Fig. 6. Linearity error of Taillefer VCDU and proposed VCDU.

resolution is the same with the forced mismatch. Careful layout should ensure that the mismatch between R_1 and R_2 is kept below 1%.

The performances of the proposed architecture is summarized in Table I and compared with some reported VCDUs. In order to compare VCDU performances, we propose the following figure of merit (FOM):

$$FOM = \frac{P}{FS^2 \times f_s} \quad (5)$$

where P is power dissipation and f_s is the sampling frequency. The proposed FOM is in line with the commonly used FOM for ADCs [10]. Using this metric, the proposed VCDU achieves a FOM of 0.86 pJ/V².

IV. APPLICATION TO $\Delta\Sigma$ MODULATION

Wide-range linear VCDUs have many applications in TMSF such as $\Delta\Sigma$ modulators, time-to-digital converters and

TABLE I. PERFORMANCE SUMMARY AND COMPARISON.

	[4]	[8]	Proposed
Conversion gain G_ϕ	-92 ps/V	-250 ps/V	-311 ps/V
8-bit linear range FS	0.82 V - 1.2 V	-0.1 V - 0.1 V	0.15 V - 1 V
Max. sampling freq. f_s	1 GHz	7.5 GHz	500 MHz
Power consumption P	175 μ W	4 mW	315 μ W
FOM [pJ/V ²]	1.22	13.33	0.86

Simulation results are obtained at the maximum sampling frequency.

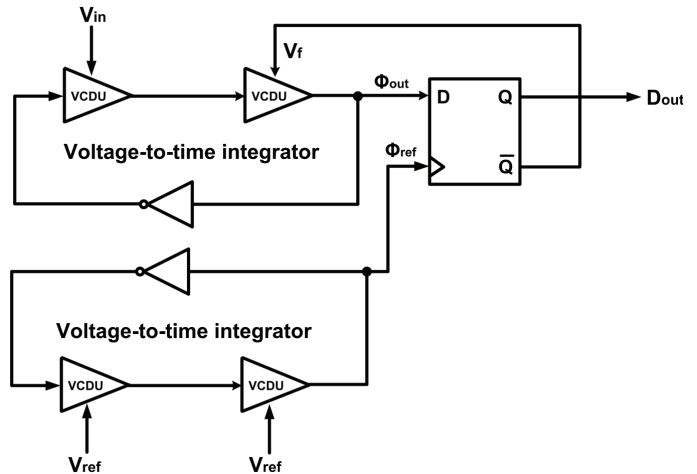


Fig. 7. First-order single-bit time-mode $\Delta\Sigma$ modulator [4].

digital phase-locked loops. In this section, the simulation of a time-mode $\Delta\Sigma$ modulator using the proposed VCDU is performed to evaluate its performance for this application.

The modulator introduced in [4] employs a VCDU in a time-mode ADC implementation with first-order noise shaping. The authors in [4] suspected that the VCDU linearity might be the limiting factor for the signal-to-noise and distortion ratio (SNDR) performances.

The modulator is realized by two voltage-controlled ring oscillators, a D flip-flop, and some digital inverters, as shown in Fig. 7. The top ring oscillator converts the input signal to a time-difference information and adds it to the inverse of the digital output. The frequency of the bottom voltage-to-time integrator (reference oscillator) is controlled by the reference voltage V_{ref} to provide the sampling frequency. The D flip-flop is a one-bit quantizer to convert the time difference between the input and the reference oscillators to a digital representation.

The differential equation between the output and input of this modulator is given by:

$$V_{out}[n] = V_{in}[n-1] + \frac{1}{G_\phi} (\Delta T_\epsilon[n] - \Delta T_\epsilon[n-1]) \quad (6)$$

where G_ϕ is the voltage-to-time conversion gain and $\Delta T_\epsilon[n]$ is the quantization error made by the D flip-flop.

This $\Delta\Sigma$ modulator was designed and simulated using Cadence Spectre in 0.18 μ m CMOS technology using the proposed VCDU. The modulator operates over a range of input voltage from 0.15 V to 1 V. The signal ring oscillator is biased at a DC offset of 0.6 V with 400 mV peak-to-peak amplitude for a 111 kHz sinusoid input signal. The reference voltage of the bottom voltage-to-time integrator V_{ref} is set to 1V to

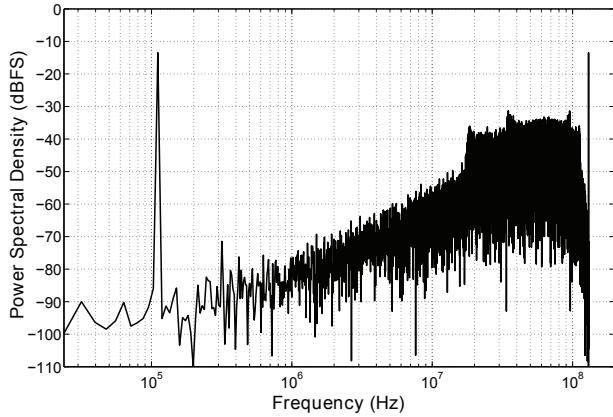


Fig. 8. PSD of the first-order $\Delta\Sigma$ modulator using the proposed VCDU.

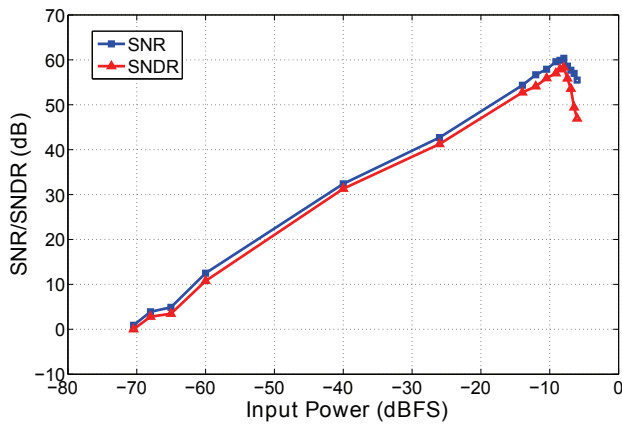


Fig. 9. SNR/SNDR versus input power.

provide a 140 MHz sampling frequency. The signal bandwidth is 400 kHz, yielding an oversampling ratio of 175.

Fig. 8 plots the power spectral density (PSD) of the modulator's output using the proposed VCDU, showing the 111 kHz input signal and first order noise shaping. The spur at 317 kHz is not an harmonic of the input signal caused by nonlinearity; it is caused by periodic quantization noise of the first order $\Delta\Sigma$ modulator. This spur, which could be removed by dithering, actually limits the SNDR of the modulator.

The signal-to-noise ratio (SNR) and SNDR versus input amplitude of the modulator are plotted in Fig. 9. These simulation results show that the peak SNR is 60 dB and peak SNDR is 58 dB. In comparison, the single-ended modulator in [4], also using $0.18\mu\text{m}$ CMOS technology, the same bandwidth and sampling frequencies, achieves a peak SNDR of 42 dB, thereby confirming that by increasing the VCDU linearity,

improved performances are obtained for the time-mode $\Delta\Sigma$ modulator.

V. CONCLUSION

A new design of a VCDU with signal conditioning is proposed which provides a wider linear range than previously published VCDUs. The circuit-level simulations confirm that the proposed architecture is linear from 0.15 V to 1 V with an equivalent 8-bit linearity error ($\pm 0.2\%$). The obtained voltage-to-time conversion gain is -311 ps/V and its power consumption is $315\ \mu\text{m}$ being supplied by a 1.8 V source. This makes it suitable for time-to-digital conversion application and analog-to-digital conversion of built-in self-test circuits, operating at low supply voltages. The performance which can be expected from this VCDU are confirmed by simulations in an example application of time-mode $\Delta\Sigma$ modulation, showing a 16 dB peak SNDR improvement over a previously reported design.

ACKNOWLEDGMENT

This work has been supported by the Natural Sciences and Engineering Research Council of Canada (NSERC). Thanks are also due to ReSMiQ for the partial support to this project.

REFERENCES

- [1] K. Bult, "Analog design in deep sub-micron CMOS," in *Solid-State Circuits Conference, 2000. ESSCIRC'00. Proceedings of the 26th European*. IEEE, 2000, pp. 126–132.
- [2] A.-J. Annema, B. Nauta, R. van Langevelde, and H. Tuinhout, "Analog circuits in ultra-deep-submicron CMOS," *Solid-State Circuits, IEEE Journal of*, vol. 40, no. 1, pp. 132–143, 2005.
- [3] M. Ali-Bakhshian and G. W. Roberts, "A digital implementation of a dual-path time-to-time integrator," *Circuits and Systems I: Regular Papers, IEEE Transactions on*, vol. 59, no. 11, pp. 2578–2591, 2012.
- [4] C. S. Taillefer and G. W. Roberts, "Delta-sigma A/D conversion via time-mode signal processing," *Circuits and Systems I: Regular Papers, IEEE Transactions on*, vol. 56, no. 9, pp. 1908–1920, 2009.
- [5] J. A. Tierno, A. V. Rylyakov, and D. J. Friedman, "A wide power supply range, wide tuning range, all static CMOS all digital PLL in 65 nm SOI," *Solid-State Circuits, IEEE Journal of*, vol. 43, no. 1, pp. 42–51, 2008.
- [6] M. M. Guttman and G. W. Roberts, "Sampled-data IIR filtering using time-mode signal processing circuits," in *Circuits and Systems, 2009. ISCAS 2009. IEEE International Symposium on*. IEEE, 2009, pp. 2285–2288.
- [7] M. Safi-Harb, S. Mirabbasi, and M. Sawan, "A time-based technique for testing LC-tank oscillators," *Circuits and Systems I: Regular Papers, IEEE Transactions on*, vol. 59, no. 9, pp. 1849–1859, 2012.
- [8] A. R. Macpherson, "A time-based 5GS/s CMOS analog-to-digital converter," *PhD thesis, University of Calgary, Canada*, 2013.
- [9] D. A. Johns and K. Martin, *Analog integrated circuit design*. John Wiley & Sons, 2008.
- [10] B. Le, T. W. Rondeau, J. H. Reed, and C. W. Bostian, "Analog-to-digital converters," *Signal Processing Magazine, IEEE*, vol. 22, no. 6, pp. 69–77, 2005.